

Supplement of Atmos. Chem. Phys., 20, 7531–7552, 2020  
<https://doi.org/10.5194/acp-20-7531-2020-supplement>  
© Author(s) 2020. This work is distributed under  
the Creative Commons Attribution 4.0 License.



*Supplement of*

## **Strong anthropogenic control of secondary organic aerosol formation from isoprene in Beijing**

**Daniel J. Bryant et al.**

*Correspondence to:* Jacqueline F. Hamilton ([jacqui.hamilton@york.ac.uk](mailto:jacqui.hamilton@york.ac.uk))

The copyright of individual parts of the supplement might differ from the CC BY 4.0 License.

## Supplementary information

### Selected Ion Flow Tube Mass Spectrometry

The data presented in this paper has been measured using a Voice200 Selected ion flow tube mass spectrometer (SIFT-MS, Syft Technologies, Christchurch, New Zealand). This instrument consists of a switchable reagent ion source capable of rapidly switching between multiple reagent ions. The ion source region where the reagent ions are generated in a microwave discharge, acts on an air/water mix at a pressure of approximately 440mTorr to generate the three reagent ions  $\text{H}_3\text{O}^+$ ,  $\text{NO}^+$ , and  $\text{O}_2^+$ . The reagent ions pass through an array of electrostatic lenses and the upstream quadrupole mass filter, and those not rejected by the mass filter are passed into the flow tube where they are carried along in a stream of nitrogen and selectively ionise target analytes. Gas phase data presented herein was determined using the  $\text{NO}^+$  reagent ion only. Sampling was carried out at a height of  $\sim 102\text{m}$  using a gas phase inlet consisting of 3.5m  $\frac{1}{4}$ " I.D. PFA tubing connected to a diaphragm inlet pump (KNF) at a total flowrate of 5 standard litres per minute (slpm), from which the SIFT-MS sampled approximately 2 slpm through an in house built pressure controlled inlet maintaining a consistent absolute inlet pressure of 0.5 bar. The flow tube is pumped by a 35  $\text{m}^3/\text{h}$  scroll-type dry pump (Edwards) resulting in a mass flow controlled gas flow of 25 sccm for the nitrogen carrier gas (research grade, BOC) and a sample flow of 100sccm from the pressure controlled inlet system. These flows result in a continuous total flow tube pressure of approximately 460 mTorr and a reaction time of approx 8ms (Hera et al. 2018). During the campaign, gas phase backgrounds were established through regularly overflowing the sample inlet with zero air for 5 continuous minutes every hour. This zero air was generated using an in house built generator using a palladium catalyst. Isoprene ( $\text{C}_5\text{H}_8$ ) was measured at product ion  $m/z$  68 ( $\text{C}_5\text{H}_8^+$ ) following charge transfer using the  $\text{NO}^+$  reagent ion. Span calibrations were carried out every 24 hours using a 1ppm gas standard traceable to the NPL scale.

### Fluorescence Assay by Gas Expansion

The OH radical measurements were made from the roof of the University of Leeds FAGE instrument container (Whalley et al., 2018). Two Fluorescence Assay by Gas Expansion (FAGE) detection cells were housed in a weather-proof enclosure at a sampling height of approximately 4 m. OH and  $\text{HO}_2$  radicals were detected sequentially in the first cell (the  $\text{HO}_x$  cell), whilst  $\text{HO}_2^*$  ( $\text{HO}_2$  plus any contributions from  $\text{RO}_2$ ) and total  $\text{RO}_2$  radical observations were made using the second FAGE cell (the  $\text{RO}_x$  cell) which was coupled with a flow reactor to facilitate  $\text{RO}_2$  detection (Whalley et al., 2018). A Nd:YAG pumped Ti:Sapphire laser was used to generate 5 kHz pulsed tunable UV light at 308 nm and used to excite OH via the  $\text{Q}_1(1)$  transition of the  $\text{A}^2\Sigma^+ +, v'=0 \leftarrow \text{X}^2\Pi_i, v''=0$  band. On-resonance fluorescence was detected using a gated micro-channel plate photomultiplier and photon counting. A background signal from laser and solar scatter and detector noise was determined by scanning the laser wavelength away from the OH transition (OHWAVE-BKD). For the entire campaign, the  $\text{HO}_x$  cell was equipped with an inlet pre injector (IPI) which chemically scavenged ambient OH by periodically by injecting propane into the air stream just above the FAGE inlet. The removal of ambient OH by chemical reaction provided an alternative means to determine the background signal ( $\text{OH}_{\text{CHEM-BKD}}$ ), without the need to tune the laser wavelength. By comparison with  $\text{OH}_{\text{WAVE-BKD}}$ ,  $\text{OH}_{\text{CHEM-BKD}}$  was used to identify if any OH was generated internally within the FAGE cell, acting as an interference signal. In general, good agreement between  $\text{OH}_{\text{CHEM-BKD}}$  and  $\text{OH}_{\text{WAVE-BKD}}$  was observed, with a ratio of 1.07 for the whole campaign (Woodward-Massey et al., PhD Thesis, University of Leeds, 2018). In this paper, the  $\text{OH}_{\text{CHEM}}$  observations are used. The instrument was calibrated every few days by over-overflowing the detection cell inlet with a turbulent flow of high purity humid air containing a known concentration of OH (and  $\text{HO}_2$ ) radicals generated by photolysing a known concentration of  $\text{H}_2\text{O}$  vapour at 185 nm. The product of the photon flux at 185 nm and the time spent in the photolysis region was measured before and after the campaign using  $\text{N}_2\text{O}$  actinometry (Commane et al., 2010).

## Figures

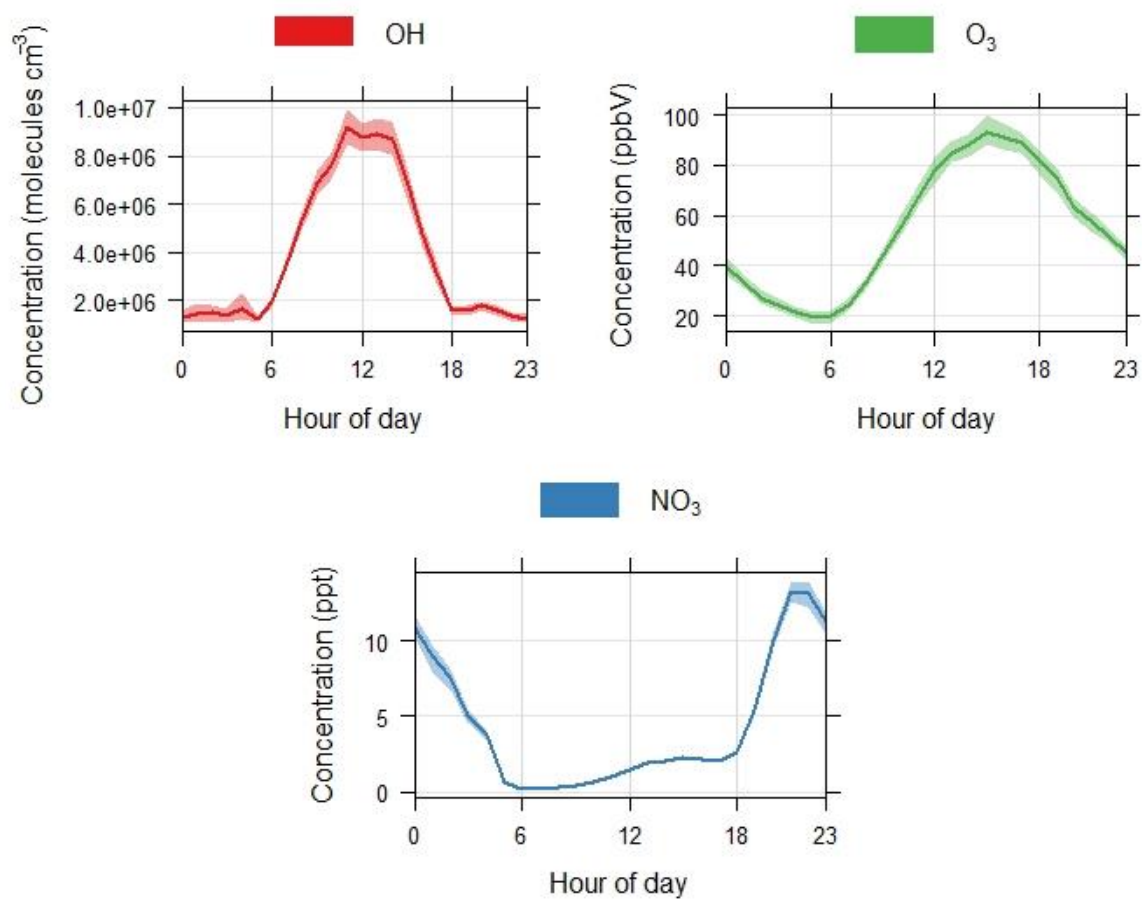


**Figure S1.** Campaign average diurnal profiles of (a) OH measured by FAGE. (b) O<sub>3</sub> measured by UV spectroscopy. (c) NO<sub>3</sub> measured by BBCEAS.

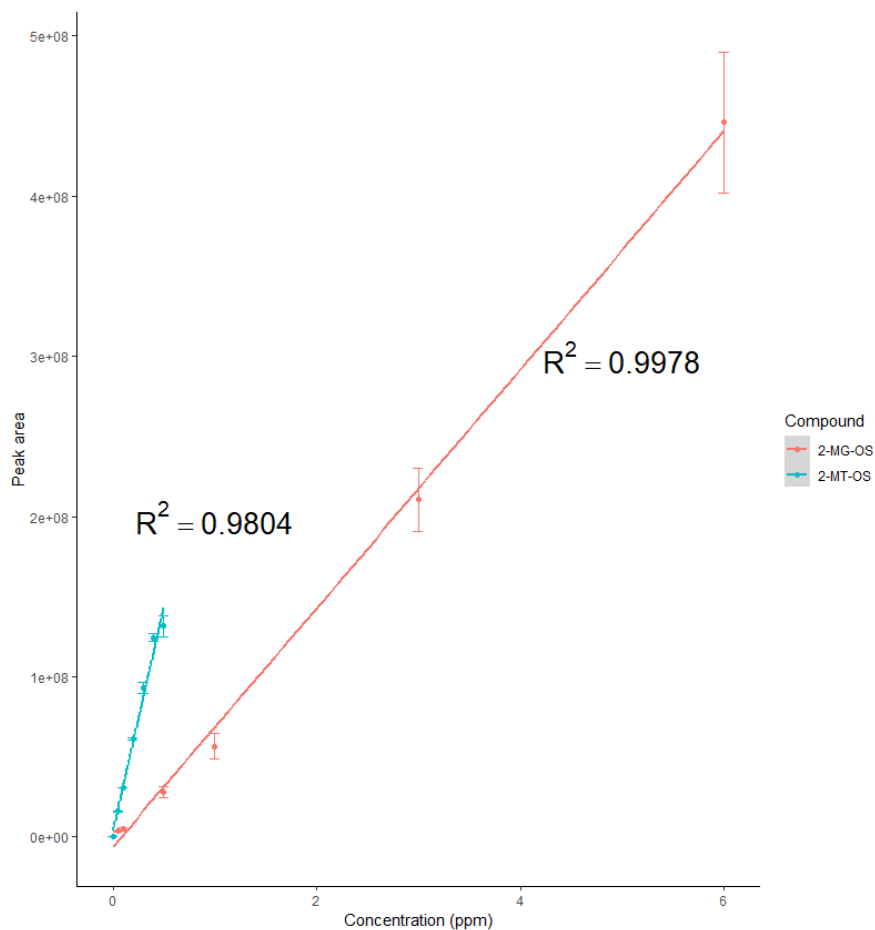


**Figure S2.** Comparison of 2-MT-OS calibration (Blue) and 2-MG-OS calibration (Red). Highlighting the difference in gradients between the two species. The error bars highlight the standard error for each concentration.

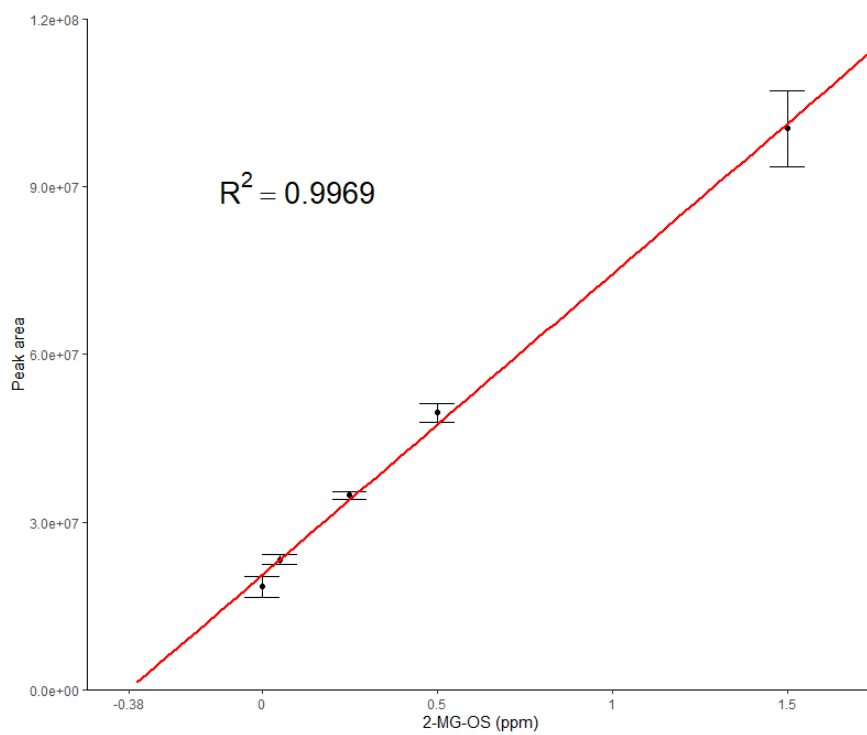


**Figure S3.** 2-MG-OS standard addition calibration of filter extract 205 in Table S2. The error bars highlight the standard error for each concentration.

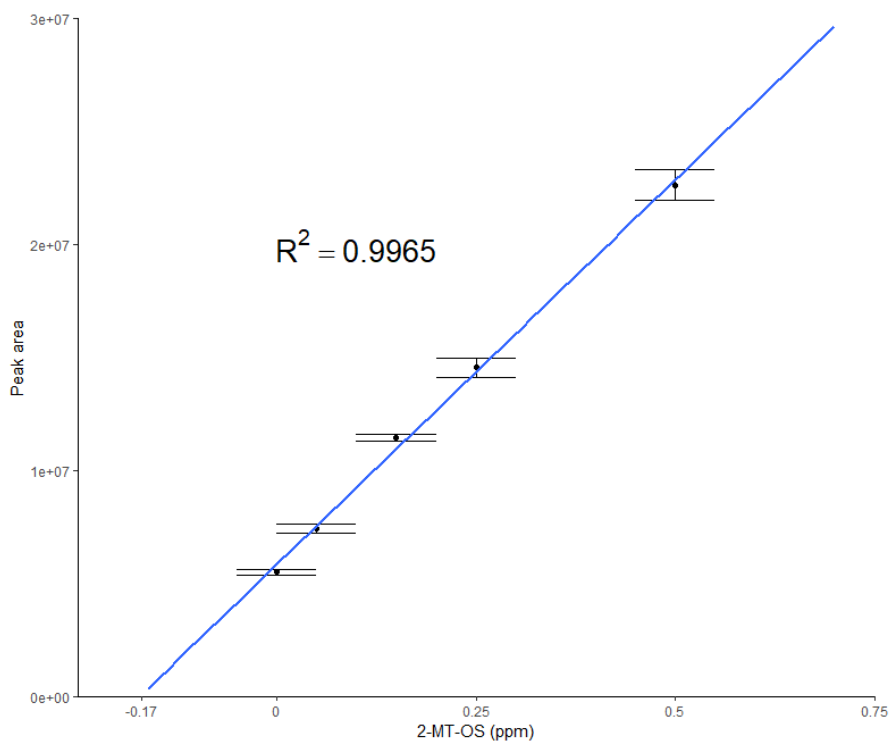


**Figure S4.** 2-MT-OS standard addition calibration of filter extract 204 in table S1. The error bars highlight the standard error for each concentration.

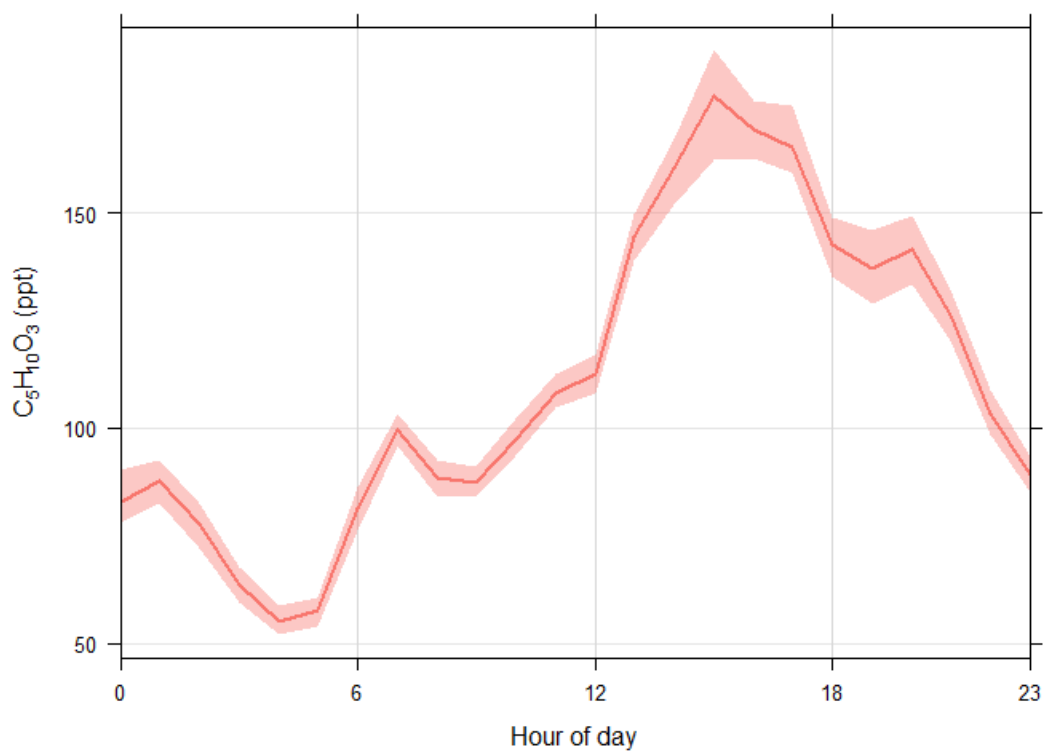


**Figure S5.** Campaign average diurnal variation with 95% confidence interval of C<sub>5</sub>H<sub>10</sub>O<sub>3</sub> measured in the gas phase using I-CIMS.



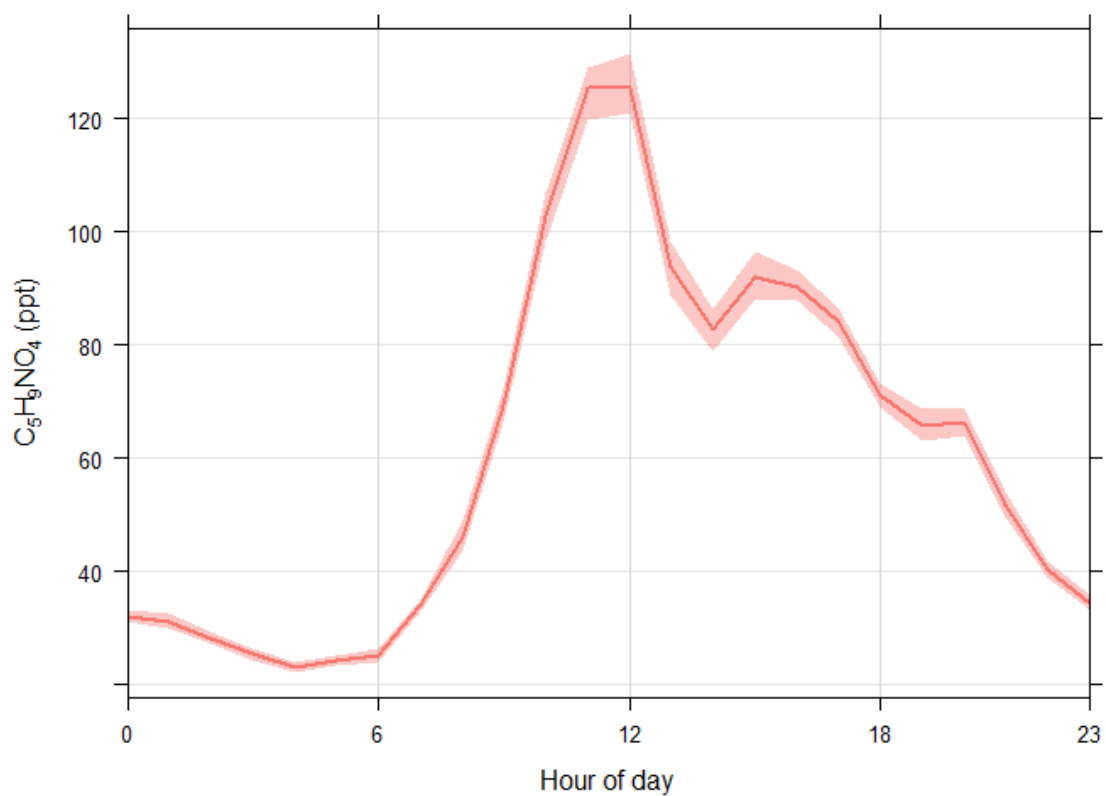


**Figure S6.** Campaign average diurnal variation with 95% confidence interval of  $C_5H_9NO_4$  measured in the gas phase using I-CIMS.

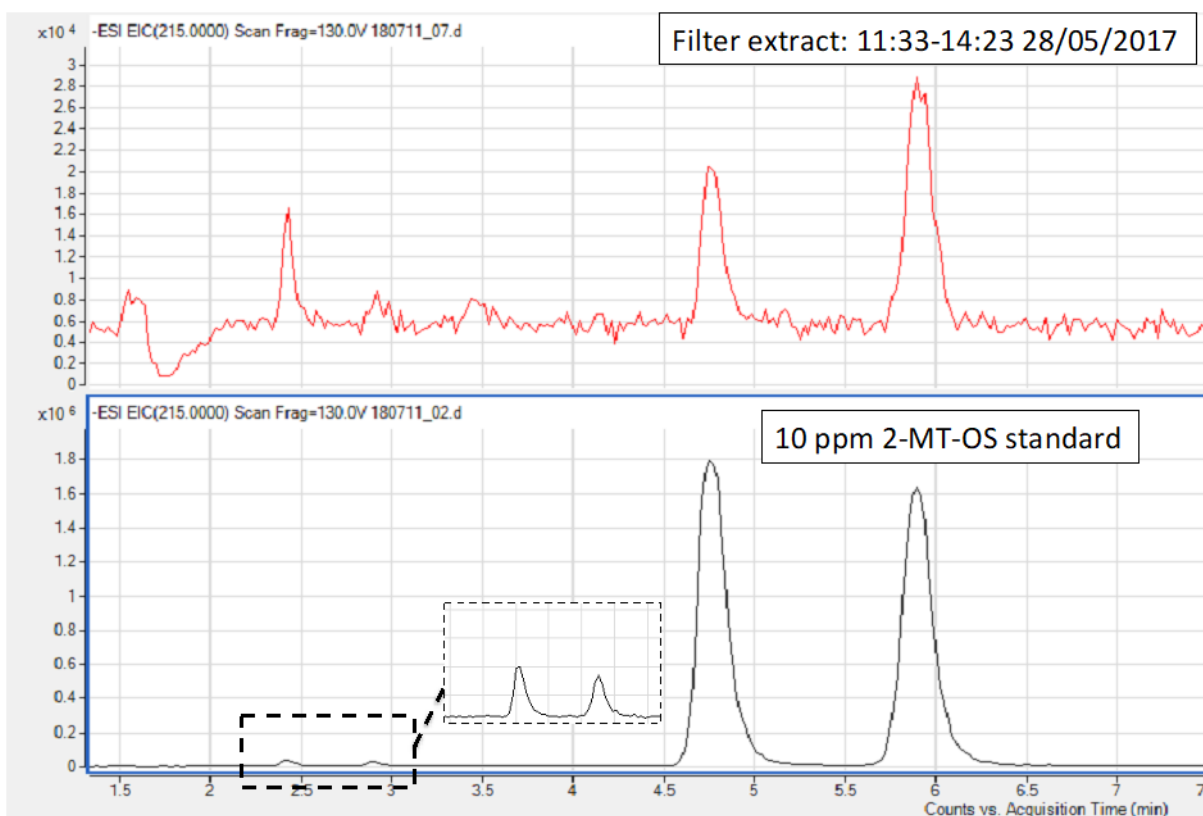


**Figure S7:** Extracted ion chromatograms ( $m/z$  215.0) using hydrophobic interaction liquid chromatography (HILIC) of 2-methyltetrol OS (2-MT-OS) isomers, highlighting improved separation of isomers using this technique. Upper: Extract of filter collected on the 28/05/2017 between 11:33 and 14:23. Lower: 10 ppm 2-MT-OS standard (Cui et al., 2018).

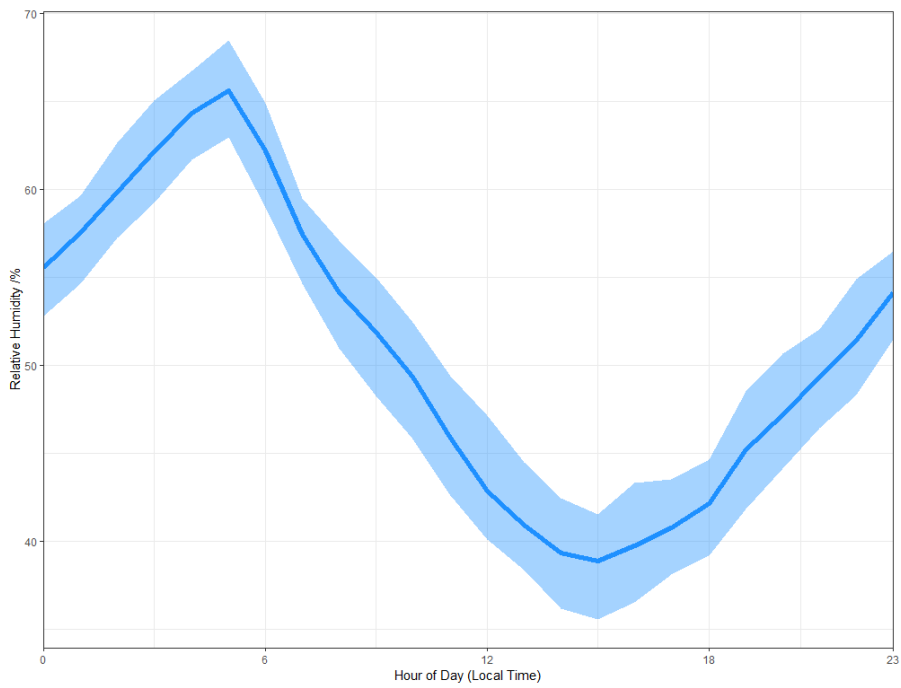


**Figure S8.** Campaign average diurnal of relative humidity (%).

**Table S1.** 2-MT-OS concentrations (ppm) for three samples (144,204,208) calculated from standard addition, 2-MG-OS and 2-MT-OS external calibrations (Fig S3).

	Filter extract concentration (ppm)			
	144	204	208	Average
Standard addition	0.078	0.17	0.18	-
External calibration (2-MG-OS)	0.03	0.07	0.07	-
External calibration (2-MT-OS)	0.009	0.06	0.02	-
Ratio of standard addition to 2-MG-OS	2.2	1.5	2.5	2.3
Ratio of standard addition to 2-MT-OS	8.6	6	10	9.2

**Table S2.** 2-MG-OS concentrations (ppm) for three samples (143,205,209) calculated from standard addition, 2-MG-OS and 2-MT-OS external calibrations (Fig S3).

Sample	Filter extract concentration (ppm)			
	143	205	209	Average
Standard addition	0.0097	0.38	0.28	-
External calibration (2-MG-OS)	0.0091	0.25	0.19	-
External calibration (2-MT-OS)	0.0023	0.064	0.049	-
Ratio of standard addition to 2-MG-OS	1.1	1.5	1.4	1.3
Ratio of standard addition to 2-MT-OS	4.2	6	5.6	5.3

**Table S3.** Collection date, start and end times for the filters analysed in this study.

Datetime	Time start	Time end
18/05/2017 15:15	13:00	17:30
19/05/2017 01:00	17:30	08:30
19/05/2017 10:06	08:40	11:32
19/05/2017 13:04	11:38	14:30
19/05/2017 16:01	14:37	17:26
20/05/2017 01:02	17:35	08:30
20/05/2017 10:04	08:40	11:29
20/05/2017 14:34	11:39	17:30
21/05/2017 01:10	17:30	08:50
21/05/2017 13:21	09:00	17:42
22/05/2017 01:06	17:50	08:23
22/05/2017 09:59	08:31	11:27
22/05/2017 13:01	11:38	14:24
22/05/2017 15:55	14:31	17:20
23/05/2017 00:52	17:30	08:15
23/05/2017 09:52	08:24	11:20
23/05/2017 12:53	11:27	14:20
23/05/2017 15:59	14:32	17:27
24/05/2017 01:05	17:33	08:38
24/05/2017 10:09	08:48	11:30
24/05/2017 13:07	11:41	14:34
24/05/2017 16:06	14:42	17:30
25/05/2017 01:04	17:40	08:29
25/05/2017 10:03	08:37	11:30
25/05/2017 13:04	11:38	14:30
25/05/2017 16:05	14:40	17:31
26/05/2017 01:06	17:40	08:33
26/05/2017 10:02	08:45	11:20
26/05/2017 12:59	11:27	14:31
26/05/2017 16:05	14:41	17:30
27/05/2017 00:57	17:40	08:15
27/05/2017 09:55	08:28	11:22
27/05/2017 12:57	11:35	14:20
27/05/2017 15:55	14:30	17:20
28/05/2017 00:57	17:31	08:24
28/05/2017 09:58	08:33	11:24

28/05/2017 12:58	11:33	14:23
28/05/2017 16:00	14:33	17:28
29/05/2017 01:03	17:40	08:26
29/05/2017 10:00	08:35	11:26
29/05/2017 13:07	11:35	14:39
29/05/2017 16:07	14:49	17:26
30/05/2017 01:00	17:35	08:25
30/05/2017 09:59	08:35	11:24
30/05/2017 12:59	11:35	14:24
30/05/2017 15:56	14:35	17:18
31/05/2017 00:55	17:30	08:21
31/05/2017 09:55	08:32	11:18
31/05/2017 12:55	11:31	14:20
31/05/2017 16:01	14:36	17:27
01/06/2017 01:05	17:37	08:33
01/06/2017 10:19	08:42	11:57
01/06/2017 13:18	12:05	14:31
01/06/2017 16:02	14:39	17:26
02/06/2017 00:59	17:34	08:24
02/06/2017 10:00	08:32	11:28
02/06/2017 13:03	11:38	14:28
02/06/2017 16:02	14:36	17:28
03/06/2017 01:03	17:35	08:31
03/06/2017 10:00	08:38	11:23
03/06/2017 12:58	11:29	14:28
03/06/2017 16:01	14:35	17:28
04/06/2017 01:03	17:38	08:28
04/06/2017 10:03	08:36	11:30
04/06/2017 13:02	11:36	14:28
04/06/2017 16:04	14:39	17:30
05/06/2017 01:03	17:38	08:28
05/06/2017 10:11	08:35	11:48
05/06/2017 13:09	11:54	14:24
05/06/2017 15:58	14:28	17:28
06/06/2017 01:05	17:34	08:37
06/06/2017 10:04	08:44	11:24
06/06/2017 13:03	11:32	14:34
06/06/2017 16:03	14:43	17:24
07/06/2017 01:03	17:32	08:34
07/06/2017 10:02	08:40	11:24
07/06/2017 12:58	11:32	14:24
07/06/2017 15:58	14:31	17:25
08/06/2017 01:00	17:32	08:29
08/06/2017 10:01	08:37	11:26
08/06/2017 12:59	11:32	14:26
08/06/2017 15:58	14:31	17:25

09/06/2017 00:57	17:30	08:25
09/06/2017 09:58	08:31	11:25
09/06/2017 12:59	11:33	14:25
09/06/2017 15:57	14:30	17:25
10/06/2017 01:39	18:49	08:30
10/06/2017 10:00	08:35	11:25
10/06/2017 12:59	11:31	14:27
10/06/2017 15:58	14:32	17:25
11/06/2017 01:04	17:31	08:37
11/06/2017 09:02	08:41	09:24
11/06/2017 09:57	09:32	10:23
11/06/2017 10:56	10:29	11:23
11/06/2017 11:56	11:30	12:23
11/06/2017 12:56	12:28	13:25
11/06/2017 13:56	13:30	14:23
11/06/2017 14:56	14:28	15:25
11/06/2017 15:57	15:30	16:25
11/06/2017 16:57	16:31	17:23
12/06/2017 01:03	17:29	08:38
12/06/2017 09:03	08:42	09:24
12/06/2017 09:56	09:29	10:24
12/06/2017 10:58	10:30	11:26
12/06/2017 11:57	11:31	12:24
12/06/2017 12:59	12:30	13:28
12/06/2017 13:57	13:32	14:23
12/06/2017 14:56	14:29	15:24
12/06/2017 15:56	15:30	16:23
12/06/2017 16:57	16:31	17:23
13/06/2017 01:04	17:30	08:38
13/06/2017 10:04	08:45	11:24
13/06/2017 12:57	11:31	14:24
13/06/2017 15:56	14:30	17:23
14/06/2017 02:26	17:30	11:23
14/06/2017 12:56	11:29	14:23
14/06/2017 15:56	14:30	17:23
15/06/2017 00:58	17:29	08:27
15/06/2017 10:01	08:36	11:27
15/06/2017 13:02	11:37	14:27
15/06/2017 16:01	14:35	17:28
16/06/2017 01:01	17:36	08:26
16/06/2017 09:59	08:33	11:26
16/06/2017 12:58	11:33	14:24
17/06/2017 08:01	07:39	08:23
17/06/2017 08:57	08:30	09:24
17/06/2017 09:57	09:30	10:24
17/06/2017 11:56	11:29	12:23

17/06/2017 12:58	12:30	13:26
17/06/2017 13:57	13:32	14:23
17/06/2017 14:55	14:28	15:23
17/06/2017 15:56	15:29	16:23
17/06/2017 17:53	17:23	18:24
18/06/2017 01:32	18:30	08:34
18/06/2017 09:04	08:45	09:23
18/06/2017 11:02	10:40	11:25
18/06/2017 15:00	14:36	15:24
18/06/2017 15:58	15:30	16:26
19/06/2017 01:03	17:30	08:36

## References

- Cui, T., Zeng, Z., dos Santos, E. O., Zhang, Z., Chen, Y., Zhang, Y., Rose, C. A., Budisulisyiorini, S. H., Collins, L. B., Bodnar, W. M., de Souza, R. A. F., Martin, S. T., Machado, C. M. D., Turpin, B. J., Gold, A., Ault, A. P., and Surratt, J. D.: Development of hydrophilic interaction liquid chromatography (HILIC) method for the chemical characterization of water-soluble isoprene epoxydiol (IEPOX)-derived secondary organic aerosol, *Environ. Sci.*, 20, 1524-1536, <https://doi.org/10.1039/c8em00308d>, 2018.
- Hera, D., Langford, V. S., McEwan, M. J., McKellar, T. I., and Milligan, D. B.: Negative Reagent Ions for Real Time Detection Using SIFT-MS, *Environments.*, 4, 16, <https://doi.org/10.3390/environments4010016>, 2017.
- Whalley, L. K., Stone, D., Dunmore, R., Hamilton, J., Hopkins, J. R., Lee, J. D., Lewis, A.C., Williams, P., Kleffmann, J., Laufs, S., Woodward-Massey, R., Heard, D. E.: Understanding in situ ozone production in the summertime through radical observations and modelling studies during the Clean air for London project (ClearfLo). *Atmos. Chem. Phys.*, 18, 2547-2571, <https://doi.org/10.5194/acp-18-2547-2018>, 2018.
- Woodward-Massey, R., Observations of radicals in the atmosphere: measurement validation and model comparisons, PhD Thesis, <http://etheses.whiterose.ac.uk/22164/>, 2018.
- Xu, L., Kollman, M. S., Song, C., Shiling, J. E., and Ng, N. L.: Effects of NO<sub>x</sub> on the volatility of secondary organic aerosol from isoprene photooxidation, *Environ. Sci. Technol.*, 48, 2253-2262, <https://doi.org/10.1021/es404842g>, 2014.
- Commane, R., Floquet, C. F. A., Ingham, T., Stone, D., Evans, M. J., and Heard, D. E.: Observations of OH and HO<sub>2</sub> radicals over West Africa, *Atmos. Chem. Phys.*, 10, 8783-8801, <https://doi.org/10.5194/acp-10-8783-2010>, 2010.